Effect of solidification cooling rate on the fatigue life of A356.2-T6 cast aluminium alloy

B. ZHANG, W. CHEN[1] and D. R. POIRIER

The Department of Materials Science and Engineering, and [1]The Department of Aerospace and Mechanical Engineering, The University of Arizona, Tucson, AZ 85721, USA

Received in final form 19 February 2000

ABSTRACT The effect of the cooling rate during solidification on the fatigue life of a cast aluminium alloy (A356.2-T6) is examined. The fatigue lives were determined for specimens removed from ingots with a gradient in cooling rates along their heights. Low- and high-cycle fatigue tests were conducted under both axial loading and reciprocating-bending conditions at a stress (strain) ratio (R) of -1.0, 0.1 and 0.2. Results show that the fatigue life decreases by a factor of three in low-cycle fatigue ($R = -1.0$) and by a factor of 100 in high-cycle fatigue ($R = 0.1$) as solidification cooling rate decreases from ~ 10 to $\sim 0.3\ \mathrm{K\,s^{-1}}$, as indicated by measurements of the secondary dendrite arm spacings in the ingots. Fatigue cracks initiated from porosity in the material solidified at slower cooling rates. When pore size is below a critical size of $\sim 80\ \mu\mathrm{m}$, as a result of increasing the cooling rate, the fatigue cracks initiated from near-surface eutectic-microconstituent. When present at or near the surface, large oxide inclusions initiated fatigue cracks.

Keywords cast aluminium; fatigue life; cooling rate; secondary dendrite arm spacing; crack initiation; microporosity.

INTRODUCTION

Aluminium castings have great potential as replacements for ferrous castings and fabrications in automobiles and rail vehicles, thereby reducing the overall weight of the vehicles for higher energy efficiency. Also, the application of aluminium castings in aerospace structures can result in significant cost reductions in aircraft manufacturing. In fact, aluminium castings are already being used for making components of these transportation vehicles; e.g. see Nath[1] for a summary of automotive applications. The potential weight and cost savings have not been fully utilized, however, because of a lack of complete understanding of the fatigue behaviour of the cast alloys. This paper presents a systematic experimental investigation of the effects of the sizes of microstructural constituents, as controlled by cooling rate during solidification on the fatigue behaviour of a cast and heat-treated aluminium alloy, A356.2-T6 (Al–7Si–0.3Mg). It builds on results that we reported in previous conference papers on the subject.[2,3]

Correspondence: W. Chen. Fax: +520 621 8191.
E-mail: weinong@u.arizona.edu

As presented in Flemings,[4] the mechanical properties of aluminium castings have been related to microstructural aspects and processing since the late 1940s. The important microstructural details of the as-cast state appear to be secondary dendrite arm spacing, porosity, inclusions, intermetallic particles, grain size, and perhaps, microsegregation. One way to control the sizes of micro-constituents in a sand-mould casting is by preferentially extracting heat to promote more rapid solidification near a 'chill'. Flemings[4] found that the dendrite arm spacing of cast structures usually correlates far better with mechanical properties than does grain size. The secondary dendrite arm spacing (SDAS) reflects the processing to the extent that increasing the cooling rate during solidification reduces SDAS, and an improvement in mechanical properties usually accompanies the reduction. Oswalt and Misra[5] used the measurement of the secondary dendrite arm spacing as a test to evaluate the tensile properties of A356 and A357 castings.

The fatigue properties of cast aluminium alloys have not been measured and studied to the extent of the

multitude of studies on tensile properties. In a study of fatigue in an Al–7Si–0.5Mg cast alloy by Pitcher and Forsyth,[6] it was found that the fatigue performance was poor, although fatigue crack propagation was slower than in high-strength wrought aluminium alloys. The primary reason was that the initiation period of the crack was very short due to the presence of defects. A study on Al–5% Cu[7,8] alloy also showed a low rate of fatigue crack propagation compared to wrought alloys. It is widely believed that most fatigue cracks in aluminium castings initiate from shrinkage pores at or close to the specimen surface,[9,10] although oxide inclusions and oxide skins have also been targeted as culprits for initiating fatigue cracks.[1,11]

In this study, to gain a better understanding of the relationship between microstructures in an aluminium casting alloy and its fatigue behaviour, we conducted experimental research on the effect of cooling rate during solidification on the sizes of microstructural features (micropores and secondary dendrite arm spacings) on the fatigue life of A356.2-T6. A mould, in which the cooling rate during solidification varied along the height of a casting-ingot, was used to effect the variation of secondary dendrite arm spacings. Specimens removed from the ingots were fatigue tested in cyclic axial loading, as well as in reciprocating-bending. Microstructural characterization and fractography were performed on the samples recovered after mechanical testing.

EXPERIMENTAL PROCEDURES

Casting

The permanent mould used to cast the A356.2 ingots is shown in Fig. 1(a). The mould was wrapped in ceramic wool, and direct water-cooling was imposed at the bottom surface. The cooling rate during solidification varied from $\sim 10\ \mathrm{K\,s^{-1}}$ at the bottom to only $0.3\ \mathrm{K\,s^{-1}}$ at ~ 150 mm from the bottom-chill. Therefore, a wide variation in cooling rates and, hence, secondary dendrite arm spacings was obtained in a single ingot. The ingots were 95 mm wide, 28 mm deep and 300 mm high. The chemical composition of the alloy is listed in Table 1. In preparation for casting, the alloy with 0.10% Ti was melted, heated to 715 °C and flux-degassed with Ar for

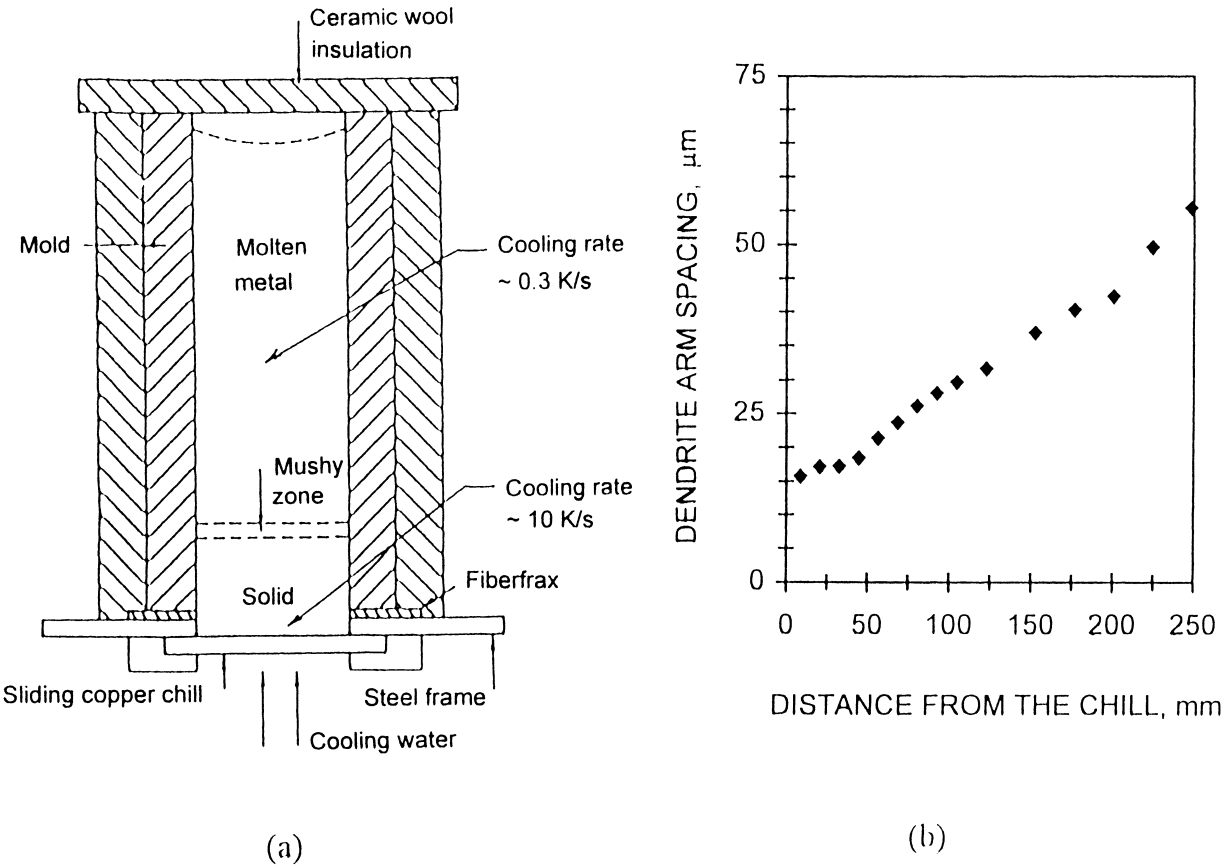

Fig. 1 The mould and secondary dendrite arm spacings: (a) the mould used for casting the aluminium alloy with a wide range of cooling rates during solidification; and (b) the resultant secondary dendrite arm spacing along its height.

Table 1 Composition of Al–7Si–0.3Mg (A356.2)

Element	Si	Fe	Mg	Ti	B	Cu	Sr	Al
Wt%	6.87	0.03	0.36	0.10	0.0001	0.01	0.006	Remainder

8 min. A small amount of additional grain refiner (Al–3Ti–1B) at 0.003% Ti level and Al–15Sr modifier at 0.008% Sr level were added 2 min prior to the end of fluxing. The cooling water was actuated before the melt was poured into the mould, which was tilted during pouring to reduce turbulence. The bottom copper chill-plate was removed 20 s after pouring, leaving cooling water directly impinging against the ingot bottom surface (i.e. the chill-surface). The resulting secondary dendrite arm spacing was $\sim$15 μm near the chill-surface and more than 50 μm in the top portion of the ingot [Fig. 1(b)].

Specimen preparation

The ingots were cut into slices, 4 mm thick, with the flat surfaces of each slice parallel to the bottom surface of the casting-ingot. A portion of each slice was kept in its as-cast state for documenting the microstructures of the as-cast alloy. The slices were then heat-treated to the T6 condition (540 °C for 12 h, quenched into water at less than 71 °C, and aged within 2 h at 155 °C for 4 h). The heat-treated slices were then milled to a thickness of 3 mm, while maintaining a depth of cut less than 0.3 mm per pass. The configurations of axial and bending fatigue specimens were then machined from the slices (Fig. 2) and polished using silicon carbide abrasive papers and alumina paste to a final finish of 0.2 μm. The direction of the final polishing operation was along the specimen length, in order to eliminate possible stress concentration sites.[12]

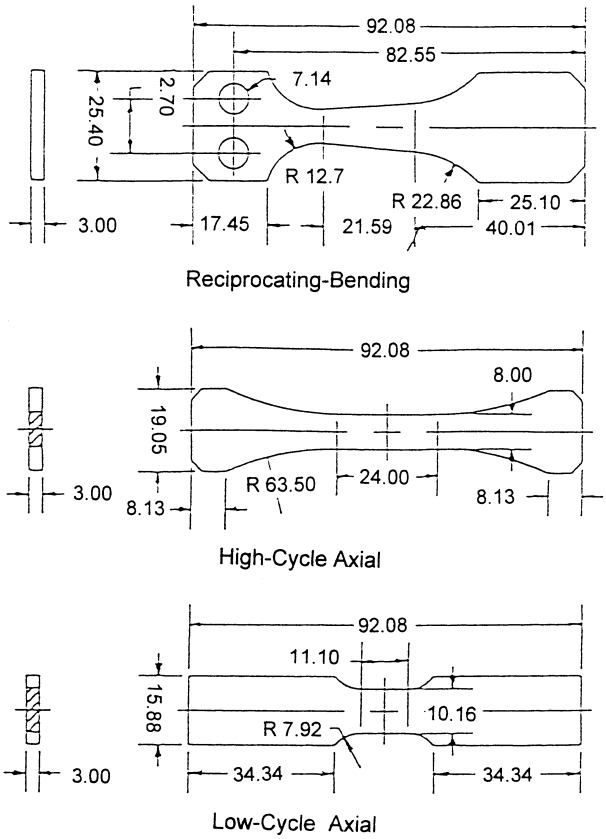

Fig. 2 Specimen geometries used in fatigue testing (all dimensions in mm).

Reciprocating-bending fatigue experiments

The bending fatigue experiments were conducted on polished specimens in a laboratory environment. The loading frequency was set at 20 Hz for strain ratios (R) of -1.0 (complete reversal) and 0.15, and at 25 Hz for $R = 0.1$. A strain gauge was attached to the centre of the gauge section of each specimen to record the cyclic strain during the test. Restricted by the ingot size, the specimens used in this research were smaller than commonly used.[12] In order to ensure a uniform strain distribution in the gauge section, finite element analysis was performed, and many trial tests were conducted using specimens of slightly different geometries taken from a wrought aluminium alloy (5052). The final geometry is shown in Fig. 2 as the reciprocating-bending specimen. In experiments with the 5052 specimens machined to the final geometry and tested in the low-cycle fatigue range, multi-fatigue cracks propagated simultaneously within the gauge sections of the specimens, which indicated that a uniform strain state in the gauge section had, indeed, been achieved. A digital-storage oscilloscope was used to record the strain data from the axially mounted strain gauge. During the experiments with the strain ratio R of -1.0, the crank-tip deflection of the test machine was adjusted to obtain a maximum strain of 0.004 for low-cycle fatigue and a maximum strain of 0.0016 for high-cycle fatigue. In order to characterize the fatigue crack initiation from the fracture surface, a strain ratio of 0.1 was also used in the high-cycle fatigue experiments and 0.15 in the low-cycle experiments to avoid the extent of damage on the fracture surfaces when the applied strain was completely reversed. The maximum strain was kept at the same level as in the case of reversed bending for high-cycle fatigue

(0.0016). The maximum strain was increased to 0.0082 to achieve $R = 0.15$ and a fatigue life in the low-cycle range.

Axial fatigue experiments

Low-cycle, constant-amplitude fatigue tests were conducted in a laboratory environment using a closed-loop servo-hydraulic testing system (Materials Test System MTS 810) in displacement control mode. High-cycle fatigue tests were conducted using the same system in load-control mode. The frequency was set at 10 Hz for low-cycle fatigue and 20 Hz for high-cycle fatigue. The specimen geometries for axial low- and high-cycle tests were designed according to ASTM Standards E606-92 and E466-82, respectively, and are shown in Fig. 2 as high-cycle and low-cycle axial specimens. The strain ratio for low-cycle fatigue was set to -1.0 (complete reversal); the strain amplitude was 0.0047. In the high-cycle fatigue experiments, the stress ratios were 1.0, 0.1 and 0.2, with the maximum/minimum stresses set to 85/−85 MPa, 175/17.5 MPa and 130/26 MPa, respectively. The high-cycle stress levels were far below the 0.2% yield strength of ~220 MPa for the alloy.

Microstructural characterization and radiography

Light microscopy was conducted to examine specimens with as-cast microstructures to determine the secondary dendrite arm spacing (SDAS), which was measured by the line-intercept method. For fractography, a sample that contained the fracture surface of the dominant fatigue crack was removed from each specimen that failed during fatigue testing. Examination of the fracture surfaces using scanning electron microscopy (SEM) revealed the fatigue crack initiation sites.

Radiographs were taken of the polished fatigue specimens, which were 3 mm thick, to reveal porosity. The radiographic unit has a tungsten target with an effective focal spot of 2.0 mm. The size of the largest pore visible on the radiographs was measured with an optical microscope at a magnification of 40×.

RESULTS AND DISCUSSION

Effects of cooling rate on SDAS and porosity

Secondary dendrite arm spacing as a function of the height along the as-cast ingot is presented in Fig. 1(b). The SDAS increases only slightly from 15 μm near the bottom-chill to 20 μm at 50 mm from the chill. As the height increases from 50 to 200 mm, SDAS increases in a nearly linear manner, with a slope of 0.15 μm/mm. Beyond 200 mm, where the cooling rate is $<0.3\ \mathrm{K\,s^{-1}}$ during solidification, SDAS is larger than 45 μm. Because the thickness rarely exceeds 75 mm in permanent mould castings [which corresponds to the microstructures with a SDAS of less than ~25 μm according to Fig. 1(b)], it is of more practical importance for automotive castings to consider the fatigue behaviour where the SDAS is less than ~25–30 μm.

Figure 3 shows the variation of the maximum length of the pores visible on the radiographs at a magnification of ~40×. Porosity was not clearly visible on the radiographs under the light microscope when the SDAS was less than 29 μm. Porosity was evident with reasonably clear boundaries at a length of ~80 μm, and the maximum length of the pores increased rapidly with increasing SDAS, as shown in Fig. 3. For example, when the SDAS is 40 μm, the maximum length of the pores, visible in the radiographs, is ~400 μm.

Fatigue life

The variation of bending fatigue life as a function of SDAS is summarized in Fig. 4. Under low-cycle fatigue conditions at $R = -1.0$, the fatigue life was $\sim 10^4$ cycles when the secondary dendrite arm spacing is 15 μm, near the bottom-chill where the cooling rate during solidification is $10\ \mathrm{K\,s^{-1}}$. The life decreases only slightly as SDAS increases to 30 μm, and the life then decreases to $\sim 3 \times 10^3$ cycles as SDAS increases to ~55 μm in the upper part of the ingot, where the cooling rate during solidification is less than $0.3\ \mathrm{K\,s^{-1}}$. The specimen with a SDAS of 53 μm had a fatigue life of only 200 cycles. An examination of the fracture showed that crack initiated at a large oxide inclusion near the surface. In the case of $R = 0.15$, the fatigue life fluctuates at $\sim 2 \times 10^4$ cycles when SDAS is <30 μm and drops to $\sim 8 \times 10^3$ cycles when SDAS is >30 μm.

Under high-cycle fatigue with $R = -1.0$, the fatigue life decreases from ~1.5 million cycles at SDAS <30 μm

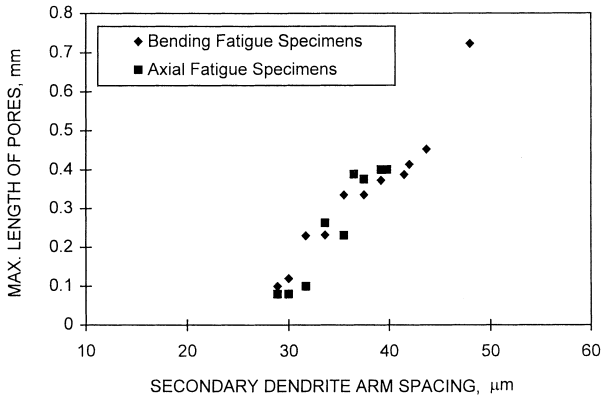

Fig. 3 Variation of pore size, visible on radiographs, with secondary dendrite arm spacing.

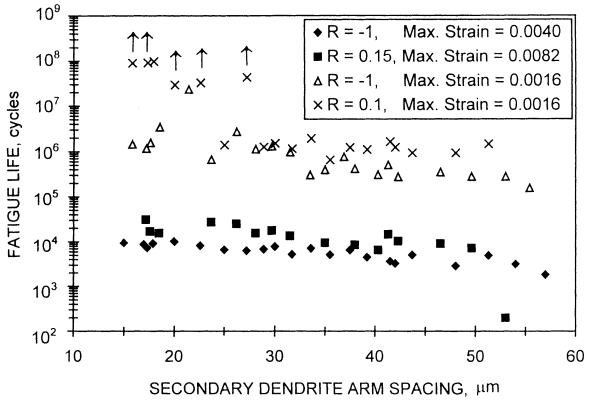

Fig. 4 Variation of bending fatigue life with secondary dendrite arm spacing. Arrows indicate specimens for which the tests were terminated before failure. Low-cycle fatigue specimens have fatigue lives of less than 10^5 cycles; high-cycle fatigue specimens have fatigue lives greater than 10^5 cycles.

to 2×10^5 cycles at SDAS of 55 μm. When the strain ratio was set to 0.1, while maintaining the maximum strain value at the same level (0.0016) as the high-cycle condition, the fatigue life of specimens with SDAS <27 μm exceeded 30×10^6 cycles without failures and no observable damage. Three specimens with SDAS of 16–18 μm lasted for almost 10^8 cycles; two of the three did not fail. The specimen with a SDAS of 25 μm failed at just over 1 million cycles, however. This specimen contained a large oxide inclusion on the surface, which initiated the fatigue crack prematurely. The fatigue lives of specimens with SDAS >29 μm are between 7×10^5 and 2×10^6 cycles. These results indicate that the amplitude of the alternating strain, not just the maximum strain, significantly affects the fatigue life of the alloy.

Figure 5 summarizes the fatigue lives obtained from low- and high-cycle axial (push–pull) tests performed at a stress (strain) ratio of -1.0. The life under low-cycle fatigue decreases from an average of 6.6×10^3 cycles at

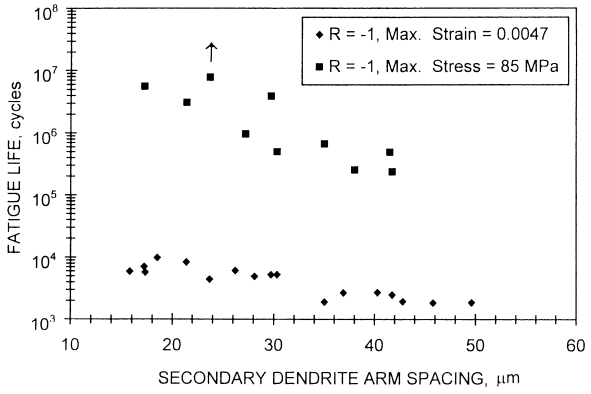

Fig. 5 Variation of fatigue life with secondary dendrite arm spacing under axial fatigue of maximum stress of 85 MPa and low-cycle fatigue with complete reversal of maximum strain of 0.0047.

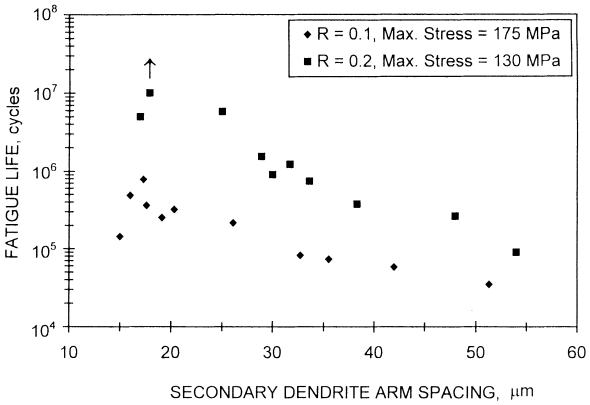

Fig. 6 Variation of fatigue life with secondary dendrite arm spacing under axial fatigue loading ($R = 0.1$ and 0.2).

SDAS <30 μm to an average of 2.6×10^3 cycles for the specimens with SDAS >35 μm. The average life under high-cycle fatigue decreases from 4.2×10^6 cycles at SDAS <30 μm to an average of 4.3×10^5 cycles at SDAS >30 μm.

Figure 6 presents the fatigue lives obtained from axial (push–pull) tests performed at stress ratios of 0.1 and 0.2. In order to avoid the very high number of cycles encountered in the bending tests, the maximum stresses were set to 175 and 130 MPa, respectively. As shown in Fig. 6, similar to the previous results, the fatigue life decreases with increasing SDAS. The fatigue lives of specimens tested with a stress ratio of 0.1 decrease from an average of 3.6×10^5 cycles to an average of only 4×10^4 cycles for the four specimens with SDAS $\geqslant 32$ μm. The fatigue lives of specimens with a stress ratio of 0.2 decrease from $\sim 10^7$ cycles at SDAS = 17 μm to less than 10^6 cycles for specimens with SDAS >30 μm.

Fatigue crack initiation time

In seven of the reciprocating-bending experiments, the formation of an observable fatigue crack was indicated by the monitored reduction of the strain amplitude or the peak strain; no attempt was made to observe crack initiation with light microscopy. When the oscilloscope record showed a change of the constant amplitude of cyclic strain, which indicated a relaxed strain state, then we assumed that relatively large fatigue cracks had formed. The corresponding number of cycles was taken as the crack initiation life. Figure 7 shows the crack initiation life as a percentage of fatigue life and its dependence on SDAS under high-cycle reciprocating-bending. In specimens with small SDAS (15–30 μm), fatigue cracks initiate at $\sim 75\%$ of the total life, whereas for specimens with large SDAS (>50 μm), fatigue cracks can initiate at merely 15% of the corresponding total

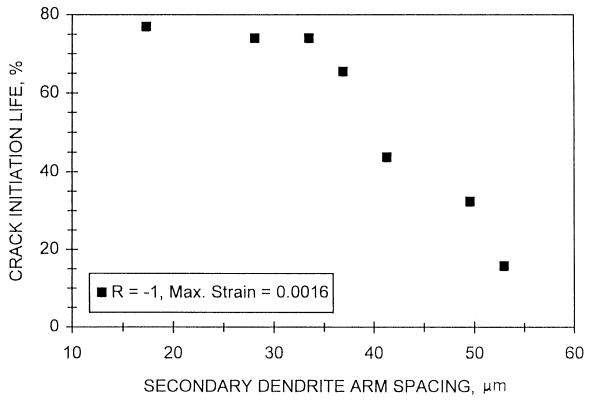

Fig. 7 Variation of crack initiation life as a percentage of total fatigue life with secondary dendrite arm spacing under reciprocating-bending.

life. This indicates that the finer microstructures obtained from the higher solidification rates significantly delayed the initiation of fatigue cracks. Such solidification rates are practically achievable in the production of automotive castings because the thickness of permanent-mould castings rarely exceeds 75 mm, and in the production of aerospace castings made in sand-moulds with strategically placed chills.

Fatigue crack initiation sites

Under both low- and high-cycle fatigue loading conditions, fatigue cracks initiated at near-surface eutectic regions in microstructures with small SDAS (<27 μm), as shown in Fig. 8. Secondary cracks were found to interact with the dominant fatigue crack, especially when

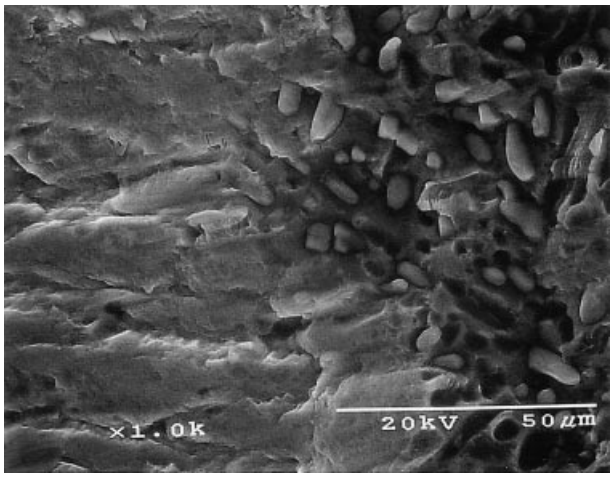

Fig. 8 Fracture surface of a low-cycle fatigue crack initiated at a eutectic constituent located at the surface (secondary dendrite arm spacing of 21 μm, 56 mm from the bottom-chill). The surface is at the right edge of the figure, and the crack propagated from right to left.

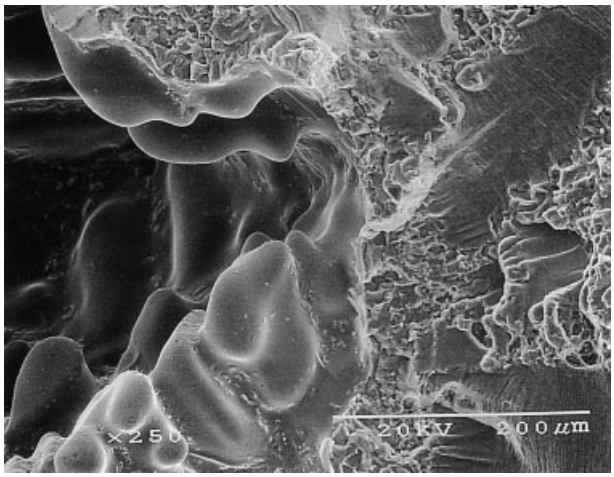

Fig. 9 Fracture surface of a low-cycle fatigue crack initiated at a pore (secondary dendrite arm spacing of 54 μm, 242 mm from the bottom-chill). The left edge of the figure is 400 μm from the surface, and the crack propagated from left to right.

the dominant crack passed through a eutectic constituent. When the SDAS >30 μm, the fatigue cracks initiated from large pores. Figure 9 shows a fatigue crack that initiated from the large pore located in the left of the figure. Similar crack initiation behaviour was observed in samples from both axial and reciprocating-bending fatigue experiments. In high-cycle bending tests (Fig. 4, $R=0.1$), the specimen with a SDAS of 25 μm failed at just over 10^6 cycles, which is much lower than the lives of neighbouring specimens. SEM examination revealed that the dominant fatigue crack was initiated by an alumina film ($\sim 100 \times 100$ μm) cutting into the specimen from its surface. Oxide-initiated cracks were also reported by others.[11,13] If pore size is used to classify the crack initiation sites instead of SDAS, based on the relationship of pore size and SDAS shown in Fig. 3, then our results indicate that fatigue cracks initiate from pores when pore size is greater than a critical value of $\sim$80–100 μm. If the pore size is below this critical value, fatigue cracks initiate from near-surface eutectic constituents. Similar critical pore sizes needed to initiate a fatigue crack in aluminium castings have been reported recently.[14]

CONCLUSIONS

The total fatigue life, under both low- and high-cycle fatigue loading conditions, of a casting aluminium alloy (A356.2-T6) has been found to be closely related to the cooling rate during solidification as quantified by secondary dendrite arm spacing. The measurement of SDAS might be used to predict the fatigue properties of this casting alloy. When SDAS is less than ~ 30 μm, the fatigue life varies slightly with SDAS under low- and

high-cycle axial and bending loading conditions. As the SDAS increases beyond 30 μm, fatigue life drops by ~3 times under low-cycle fatigue and ~100 times under high-cycle fatigue at $R = 0.1$. Fatigue cracks initiate at or near surface eutectic regions when the SDAS is less than ~27 μm. When the SDAS is greater than 30 μm, porosity becomes the dominant crack initiation site. A SDAS of 30 μm corresponds to a critical pore size of ~80–100 μm. Therefore, in the absence of oxide inclusions, pore size may also be used as a parameter to predict the fatigue behaviour of this casting alloy.

Acknowledgements

This work was supported by the US Department of Energy. The authors are grateful to Dr Q. T. Fang of Alcoa for his supervision during the production of the castings used in this research and for his insightful conversations, and to Mr P. T. Hushek, Phoenix Heat Treating, for heat-treating the specimens used in this study.

REFERENCES

1 J. Nath (1995) Process and material options for automotive chassis aluminum castings. SAE Technical Paper Series 950723. In: *Aluminum Applications for Automotive Design* (SP-1097), SAE, Warrendale, PA, pp. 75–90.
2 W. Chen, B. Zhang, T. Wu, D. R. Poirier, P. Sung and Q. T. Fang (1998) Microstructure dependence of fatigue life for A356.2. In: *Automotive Alloys II* (Edited by S. K. Das), TMS, Warrendale, PA, pp. 99–113.
3 W. Chen, B. Zhang, T. Wu, D. R. Poirier and Q. T. Fang (1998) The role of dendrite arm spacing in the fatigue of cast aluminum. In: *Advances in Aluminum Casting Technology* (Edited by M. Tiryakioğlu and J. Campbell), ASM International, Materials Park, OH, pp. 207–216.
4 M. C. Flemings (1974) *Solidification Processing*, McGraw-Hill, New York, NY, pp. 341–344.
5 K. J. Oswalt and M. S. Misra (1981) Dendrite arm spacing (DAS): a nondestructive test to evaluate tensile properties of premium quality aluminum alloy (Al–Si–Mg) castings. *AFS Int. Cast Metals Journal*, **March**, 23–40.
6 P. D. Pitcher and P. J. E. Forsyth (1982) The influence of microstructure on the fatigue properties of an Al casting alloy. Royal Aircraft Establishment, Technical Report 82107.
7 R. J. Stofanak, R. W. Hertzberg, G. Miller, R. Jaccard and K. Donald (1983) On the cyclic behavior of cast and extruded aluminum alloys, part A: fatigue crack propagation. *Engng Fracture Mech.* **17,** 527–539.
8 R. J. Stofanak, R. W. Hertzberg, J. Leupp and R. Jaccard (1983) On the cyclic behavior of cast and extruded aluminum alloys, part B: fractography. *Engng Fracture Mech.* **17,** 541–554.
9 B. Skallerud, T. Iveland and G. Harkegard (1993) Fatigue life assessment of aluminum alloys with casting defects. *Engng Fracture Mech.* **44,** 857–874.
10 M. J. Couper, A. E. Neeson and J. R. Griffiths (1990) Casting defects and the fatigue behavior of an aluminum casting alloy. *Fatigue Fract. Engng Mater. Struct.* **13,** 213–227.
11 J. Campbell, C. Nyahumva and N. R. Green (1998) The concept of the fatigue potential of cast alloys. In: *Advances in Aluminum Casting Technology* (Edited by M. Tiryakioğlu and J. Campbell), ASM International, Materials Park, OH, pp. 225–234.
12 E. J. Czyryca (1985) *Metals Handbook*, 9th edition, Vol. 8, ASM International, Materials Park, OH, pp. 366–375.
13 Q. G. Wang, D. Apelian and J. R. Griffiths (1998) Microstructural effects on the fatigue properties of aluminum castings. In: *Advances in Aluminum Casting Technology* (Edited by M. Tiryakioğlu and J. Campbell), ASM International, Materials Park, OH, pp. 217–224.
14 H. R. Mayer, H. J. Lipowsky, M. Papakyriacou, R. Rosch, A. Stich and S. Stanzl-Tschegg (1999) Application of ultrasound for fatigue testing of lightweight alloys. *Fatigue Fract. Engng Mater. Struct.* **22,** 591–600.